PAPER

Heteroatom-doped highly porous carbons prepared by *in situ* activation for efficient adsorptive removal of sulfamethoxazole†

Wei Zheng, [ID] ‡[a] Yawei Shi, [ID] ‡[a] Guozhu Liu,[b] Bin Zhao[a] and Liang Wang [ID] *[a]

Using organic salts as precursors, heteroatom-doped porous carbons prepared by *in situ* activation had surface areas of up to 2703 m^2 g^{-1}. These porous carbons have been found to be effective adsorbents for adsorption of sulfamethoxazole (SMX) from water. The effects of precursor type, calcination temperature, pH and ionic strength as well as the regeneration properties were investigated. The different adsorption performances of porous carbons were related to their textural structures and chemical properties, and a reasonable adsorption mechanism was proposed. The effects of different heteroatom functional groups on the adsorption of SMX were also analyzed in detail. For potential practical applications, the performance of the porous carbon for removing SMX from real water was also tested.

1. Introduction

Since the invention of antibiotics, they have been widely used to treat humans and animals because they can selectively kill or inhibit microorganisms. However, a large part of antibiotics cannot be metabolized by the body and are excreted in the urine and feces as the original drug, and are not easily degraded in the environment.[1] Sulfonamides are still widely used antibiotics today.[2] It is noted that due to their structural stability and environmental persistence, sulfonamides can be easily accumulated in the environment. According to previous reports,[3,4] sulfonamides have been detected in soil, sediments, surface water, groundwater and even drinking water. Sulfamethoxazole (SMX), a typical antibiotic in this category, is widely used for treatment of bacterial diseases.[5] It is therefore urgent to remove SMX contamination from the water environment.

Porous carbons have long been applied in fields including energy storage, electrical applications, catalysis and adsorption.[6–8] The conventional way to prepare porous carbons is through the typical activation method. Commonly used activation agents are NaOH, KOH, H$_3$PO$_4$, *etc.*[9] Taking KOH as an example, the commonly used mixing methods are the grinding method and the impregnation method.[10] The grinding method often has the problem of ununiform mixing. The impregnation method enables more uniform mixing of KOH and the carbon precursor. However, there was a higher energy consumption in the process of evaporating and crystallizing. Recently, there have been some reports regarding the production of porous carbon through direct carbonization of organic salts.[11,12] Those salts contain certain elements (Na or K),[13] which can produce inorganic substances that act as activation agents during carbonization. Since these elements are uniformly dispersed in the organic matrix at the molecular level, the activation process will be very effective. In addition, heteroatoms, N and O for instance, can be introduced by selecting a suitable precursor.[7,11]

Since ethylenediaminetetraacetate (EDTA) contains nitrogen, nitrogen doping can be introduced. Recently, nitrogen-doped carbons with EDTA-4Na and EDTA-2K as precursors have been prepared.[11,14] To investigate the effect of alkali metal species in the precursor of EDTA salts on the properties of the prepared carbons, a series of porous carbons were prepared from three different precursors (EDTA-2Na, EDTA-4Na and EDTA-2K) in this work. Furthermore, for the adsorption of SMX, the effects of precursor type and calcination temperature on the adsorption performance were investigated. The effects of initial concentration, contact time, pH and ionic strength as well as the regeneration property were also investigated. The different adsorption performances of porous carbons were related to their physical structure and chemical properties, and a reasonable adsorption mechanism was proposed. For potential practical applications, adsorptive removal of SMX from real water was also tested.

[a]State Key Laboratory of Separation Membranes and Membrane Processes, School of Environmental Science and Engineering, Tiangong University, Tianjin 300387, China. E-mail: mashi7822@163.com; Fax: +86 22 83955392; Tel: +86 22 83955392
[b]School of Chemical Engineering and Technology, Tianjin University, Tianjin 300072, China

† Electronic supplementary information (ESI) available. See DOI: 10.1039/c9ra09269b

‡ Wei Zheng and Yawei Shi contributed equally.

2. Experimental

2.1. Materials

EDTA-2K ($C_{10}H_{14}N_2O_8K_2 \cdot 2H_2O$), EDTA-2Na ($C_{10}H_{14}N_2O_8Na_2$) and EDTA-4Na ($C_{10}H_{12}N_2O_8Na_4$) were purchased from Macklin (Shanghai, China). Sulfamethoxazole (SMX, 99%) was purchased from Aladdin (Shanghai, China).

2.2. Preparation

For preparation of the carbon adsorbents, the organic salt (EDTA-2K, EDTA-2Na or EDTA-4Na) as the precursor loaded in a porcelain boat was carbonized in a horizontal tube furnace (Tianjin Zhonghuan). The furnace was heated to 600–800 °C by electric heating at a 5 °C min^{-1} heating rate and then maintained for 1 h in nitrogen flow, followed by cooling down to ambient temperature. The resulting power was washed with diluted hydrochloric acid (1 M) and distilled water and dried at 120 °C to obtain the carbon product, which was denoted as X-T. Here X represented the precursor type and T represented the pyrolysis temperature. For example, the adsorbent by carbonization of EDTA-2K at 700 °C was named as 2K-700.

2.3. Characterizations

The morphologies of the EDTA-salts-dervied carbons were observed by scanning electron microscope (SEM, HITACHI-S4800, Japan) and transmission electron microscope (TEM, Tecnai G2 Spirit Twin, USA). Bulk elemental compositions were tested using elemental analysis (EA, Elementar, VARIO EL cube, Germany) and the contents of oxygen were obtained by difference. The samples were subjected to an X-ray photoelectron spectroscopy (XPS, Thermofisher, America) for the determination of the surface elemental compositions. The samples were also subjected to X-ray diffraction (XRD) experiments (Bruker D8 Advance, Germany). The samples were also characterized using a Raman spectroscope (Horiba, Japan). The concentrations of SMX in deionized water were

analyzed by a UV-vis spectrophotometer at 267 nm. The concentrations of SMX in lake water were analyzed using high performance liquid chromatography (LC-20AT, Shimadzu, Japan) with a UV detector set at 267 nm. The specific surface areas and porosities were calculated from the N_2 adsorption–desorption isotherms measured at 77 K using an Autosorb-IQ-C apparatus (Quantachrome Corp., USA). Zeta potential values were measured at several pH values using 5 mg carbon in 10 mL KCl solution (1 mM) using a Nano-ZS90 (Malvern Instruments, UK).

2.4. Adsorption experiments

To evaluate the adsorption performance toward SMX from water, we conducted a series of adsorption experiments. The tests for isotherm and kinetics studies were conducted by adding 5.0 mg carbon into 100 mL SMX aqueous solutions at pH 5.0 under dark condition and then put in a water bath and stirred at a constant speed for 3 hours at 30 °C. The equilibrium adsorption amount of SMX q_e in mg g^{-1} was obtained by eqn (S1).†

The adsorption kinetics of SMX on 2K-700 were conducted in the range of 1–180 min, for 20, 50 and 100 mg L^{-1} SMX solutions at pH 5.0 and 30 °C respectively. The adsorption amount q_t in mg g^{-1} at any t time was obtained by eqn (S2).†

Effect of pH on SMX adsorption performance on 2K-700 was studied by tailoring pH of 50 mg L^{-1} SMX solutions with NaOH (0.1 M) or HCl (0.1 M). Effect of ionic strength on adsorption was tested by adding NaCl, KCl, MgCl$_2$ or CaCl$_2$. For reusability test, the spent porous carbon was washed by ethanol, then dried in an oven at 120 °C, and used again for adsorption of SMX. These test were conducted with 5.0 mg carbon and 50 mL SMX solution.

A sensitive balance ($d = 0.01$ mg, METTLER TOLEDO XS205) was used for weighing the adsorbents. All the adsorption experiments in this study were performed at least twice and the mean values with standard errors less than 5% were reported.
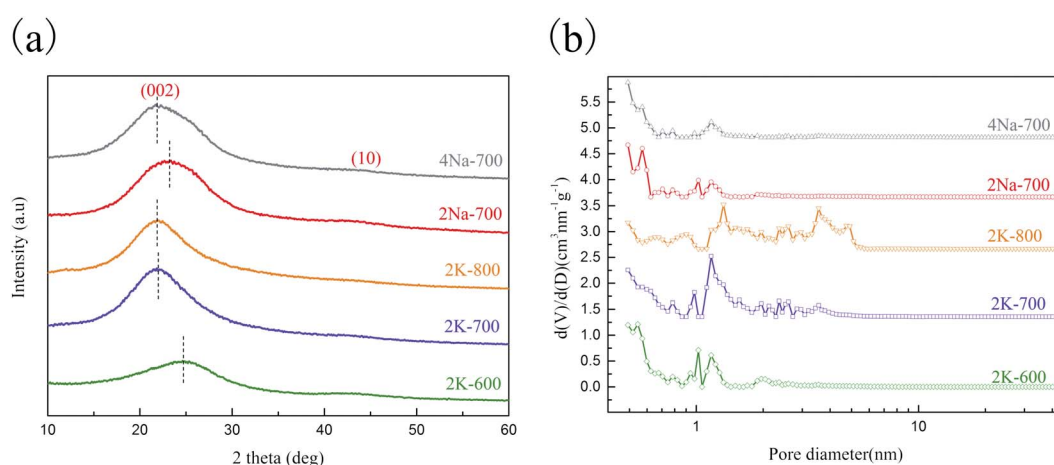

Fig. 1 XRD patters (a) and NL–DFT pore size distributions (b) of porous carbons.

3. Results and discussion

3.1. Characterization

As is shown in Fig. S1† the porous carbons derived from EDTA-2K had microscopic morphologies like the combination of cheese and microspheres, while carbons derived from EDTA-2Na and EDTA-4Na had morphologies with loosely packed irregular wedge-shaped particles. The porous carbons derived from potassium and sodium salts had obviously different surface topography, probably because of the different activation processes induced by potassium and sodium respectively. From the TEM images (Fig. S2†), irregular pores could be observed at the boundaries of porous carbon particles, which proved their porous structures.

Fig. 1a showed the XRD patterns of the porous carbons prepared at different conditions. The patterns showed two peaks at $\sim25°$ and $\sim44°$ respectively, corresponding to (002) and (100) crystal planes, indicating that all five carbon materials were amorphous.[15] Comparing 2K-600, 2K-700 and 2K-800, as the pyrolysis temperature increased, the (002) peak shifted to a smaller angle, indicating an increase in the spacing of the graphene layers.

During the carbonization of potassium organic salts,[13,16] potassium carbonate (K_2CO_3) and water could be formed *in situ*, leading to a series of reactions (reaction (S1)–(S6)†) which contributed to the *in situ* activation process.

The vapors of metallic K could be intercalated between the carbon lattices, causing swelling of the graphene layers and the formation of more defects in the carbon microstructure.[10] Reactions (S2) and (S3)† are endothermic ones. With the reaction temperature increasing from 600 to 800 °C, the reaction equilibrium moves towards the positive direction and the reaction rate increases as well, leading to more severe carbon activation and thus increased inter-layer distance as indicated by XRD measurements. For 2K-700 and 2Na-700, the ratio of alkali metal atoms to organic moieties in the precursors (EDTA-2K and EDTA-2Na) and the activation temperature were the same. However, the peak moved slightly to a smaller angle for 2K-700, indicating an increase in the layer-to-layer distance, which again showed that the activation process induced by Na and K may be different.[9] Fig. S3† showed the Raman spectra of the porous carbons prepared at different conditions. The appearance of the D (disordered graphite lattice) and G (graphite lattice) peaks indicated the amorphous structure of the porous carbons, which is consistent with the results of XRD.

The ratio of I_D/I_G increases with the increase of the pyrolysis temperature (600–800 °C), showing an increase in carbon defects.[17] This may be due to the more intense *in situ* activation as the pyrolysis temperature increases, causing the graphene layer to form more defects in the carbon microstructure.

To further investigate the diversities in properties of porous carbon prepared by sodium and potassium salts, the porosities of the carbons were characterized by measuring the nitrogen sorption isotherms (Fig. S4†).

The textural properties of the carbons were summarized in Table 1. From 2K-600 to 2K-800, a higher nitrogen adsorption uptake at p/p_0 close to zero was observed (Fig. S4†), implying the generation of more micropores. In addition, obvious widening of the isotherm knee and the appearance of a hysteresis loop was observed for 2K-800, which indicated the formation of larger pores. This was also reflected from the shift to larger pores sizes in the calculated pore size distributions in Fig. 1b. Obviously, a higher carbonization temperature favored the *in situ* activation process (reaction (S1)–(S6)†), leading to a better developed pore network in 2K-800. Comparing 2K-700 and 2Na-700, the former one had an obviously larger surface area than the latter (Table 1). Besides, the PSD results (Fig. 1b) also indicated that 2K-700 possessed larger pore sizes. The results clearly showed that potassium had a stronger pore-formation effect compared to sodium in the *in situ* activation process. This was probably attributed to the lower starting temperature of potassium related activation reactions in the carbonization process, similar to the case when KOH and NaOH were compared for carbon activation in previous reports.[18,19]

The porous carbons prepared with two different sodium salts were also compared. As shown in Table 1, 4Na-700 and 2Na-700 possessed similar surface areas and total pore volumes, but the pores in 4Na-700 were relatively larger as indicated from the PSDs (Fig. 1b). The carbonization temperatures of 2Na-700 and 4Na-700 were the same, and the ratio of Na to organic moieties in the precursor of 4Na-700 was higher. During the carbonization of 4Na-700, more sodium atoms participated in the pore-forming process. Thus, more serious etching of the pore walls in the carbon occurred, resulting in the formation of larger pores.

The bulk elemental compositions were determined by CHN elemental analysis (Fig. 2a). Nitrogen doping was observed for all the porous carbons inherited from nitrogen-rich precursors. The content of nitrogen declined from 2K-600 to 2K-800, which was attributed to the decomposition of functional groups at a higher temperature.[20,21]

XPS measurements were conducted to further investigate the heteroatom functional groups on the carbons (Fig. S5a†).[22] Fig. 2b presented heteroatom contents of the carbon samples determined by XPS. The surface compositions of porous carbons determined by XPS were very similar with the bulk contents obtained from EA, indicating that heteroatoms were uniformly doped during high temperature pyrolysis.

The deconvolution of the O1s (Fig. S5b–f†) and N 1s (Fig. S6a–e†) spectra revealed the types of oxygen and nitrogen groups (Table 2). The O 1s spectra could be fitted to three peaks at 531.1–531.6, 532.8–533.1 and 534.6–535.5 eV, which were

Table 1 Textural properties of the studied adsorbents

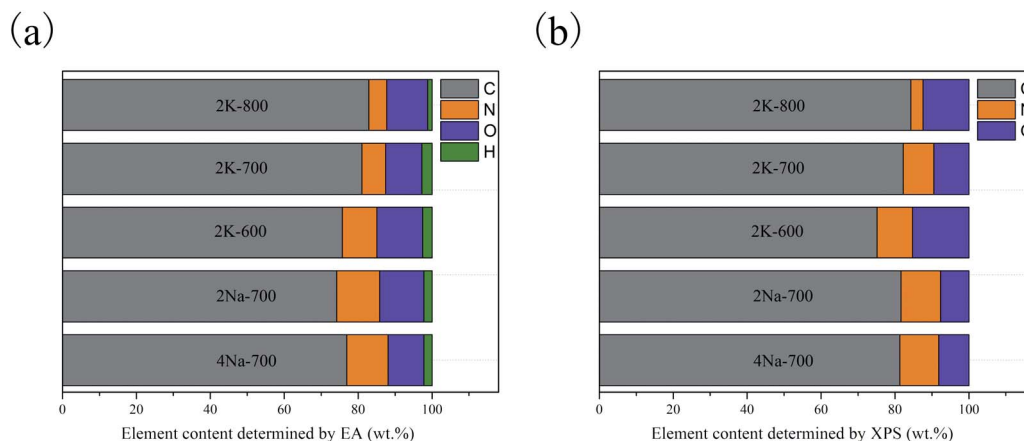| Sample	S_{BET} ($m^2 \ g^{-1}$)	V_{total} ($cm^3 \ g^{-1}$)	V_{micro} ($cm^3 \ g^{-1}$)	I_D/I_G	Yield (%)
2K-600	1186	0.593	0.325	0.925	19.6
2K-700	1739	0.939	0.489	0.968	14.9
2K-800	2703	1.701	0.433	0.992	4.9
2Na-700	680	0.344	0.159	1.027	18.2
4Na-700	617	0.364	0.139	1.037	16.8

(a)   (b)

Fig. 2   Elemental contents of porous carbons determined by elemental analysis (a) and XPS (b).

Table 2   Heteroatom contents of the porous carbons determined by XPS

Sample	Types of oxygen (at%)			Types of nitrogen (at%)			
	O-1	O-2	O-3	N-6	N-5	N-Q	N-X
2K-600	1.96	8.37	1.72	2.13	4.22	1.17	1.17
2K-700	3.65	1.96	1.78	2.12	2.73	1.09	1.44
2K-800	5.46	3.81	0.38	0.77	0.94	0.62	0.58
2Na-700	2.76	2.56	0.64	2.55	2.94	1.47	2.57
4Na-700	2.70	2.68	0.97	2.35	3.11	1.76	2.10

attributed to carbonyl groups (O-1), phenol and ether groups (O-2), and chemisorbed oxygen/water (O-3).[23–25] For N 1s spectra, binding energies at 398.5–398.7, 400.1–400.4, 401.4–402.3 and 404.7–406.3 eV were assigned to pyridinic (N-6), pyrrolic (N-5), graphitic (N-Q) and oxide nitrogen (N-X).[21,26,27] Based on the nitrogen content of each porous carbon, the contents of different nitrogen species in each sample were calculated (Table 2). As the pyrolysis temperature increases from 600 to 800 °C, the content of N-Q decreases by 47.41%, while N-6 and N-5 decrease by 63.95% and 77.80%, respectively. This indicates that N-Q with the least decomposition ratio was the most thermostable species,[21] or some N-6 and N-5 are converted into N-Q.[28]

3.2.   Effect of precursor type and activation temperature on SMX adsorption

Based on previous reports,[29,30] activation temperature and precursor type could greatly affect the adsorption performances of resulting carbons. The carbons prepared with three different precursors were employed for the adsorptive removal of SMX at a series of initial concentrations. As expected, with the SMX concentration changes from 20 to 100 mg L^{-1}, the adsorption amount increased significantly (Fig. 3). At a higher initial concentration, the driving force of molecular diffusion was increased, thereby increasing the adsorption capacity. The nonlinear fitting parameters derived from Langmuir and

Freundlich models (eqn (S3)–(S4)†) were displayed in Table 3. Both models had high correlation coefficients (R^2), indicating that the adsorption of SMX on these porous carbons could be well described by the two models.

As shown in the Fig. 3 and Table 3, the carbon adsorbents prepared from potassium and sodium salts under the same preparation conditions showed great differences in adsorption amounts towards SMX. The maximum adsorption amount of SMX (q_{max}) obtained from the Langmuir model (Table 3) for 2K-700 was significantly higher than that for 2Na-700 and 4Na-700. In the Freundlich model, K_F was the Freundlich constant indicating the adsorption capacity. The order in K_F value was consistent with the order in q_{max} calculated by the Langmuir model, further demonstrating the reliability of the data. As discussed above, the pore-forming effect of K is stronger than Na, which resulted in a better developed pore structure in 2K-700 and significantly improved the performance of 2K-700 for SMX adsorption.

Using EDTA-2K as the optimum precursor, the effect of activation temperature was further investigated. As shown in Table 3, q_{max} was gradually enhanced from 2K-600 to 2K-800. From 600 to 700 °C, increase in q_{max} was very significant, reaching 65%. However, comparing to 2K-700, q_{max} was only
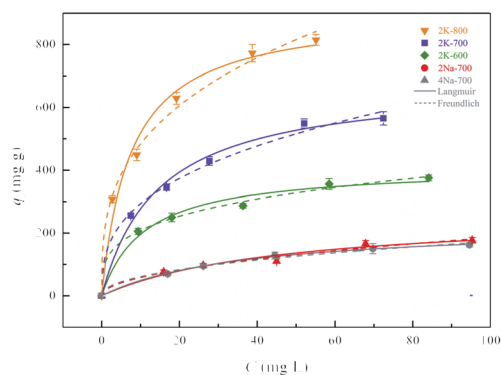

Fig. 3   The effect of precursor and pyrolysis temperature on adsorption of SMX by porous carbons.

Table 3 The fitting parameters of Langmuir and the Freundlich isotherm models

Isotherm models	Langmuir			Freundlich		
Sample	q_{max} (mg g^{-1})	K_L (L mg^{-1})	R^2	K_F ((mg g^{-1}) (L mg^{-1})$^{1/n}$)	n	R^2
2K-600	411.84	9.07×10^{-2}	0.982	109.1	3.55	0.996
2K-700	681.24	6.84×10^{-2}	0.992	130.5	2.85	0.992
2K-800	906.93	1.33×10^{-1}	0.981	228.9	3.08	0.994
2Na-700	262.49	2.16×10^{-2}	0.967	18.47	1.99	0.976
4Na-700	227.68	2.74×10^{-2}	0.998	21.55	2.21	0.987

increased by 33% for 2K-800. In addition, although 2K-800 had the largest specific surface area and pore volume, its yield was quite low (Table 1) and the production process consumed more energy. Thus, 2K-700 was selected as the optimal one for further research.

3.3. Adsorption kinetics

To study the adsorption rate and control steps of 2K-700 for SMX from aqueous solution, we carried out adsorption kinetic experiments. The nonlinear fitting in pseudo-second-order (PSO) and pseudo-first-order (PFO) models (eqn (S5)–(S6)†) at different initial concentration were shown in Fig. 4a.

During the first 30 minutes, the adsorption rate was quite rapid due to the presence of more empty active sites. After that, the adsorption rate gradually decreased until equilibrium was reached. Higher regression coefficient (R^2) values indicated that the PSO model could describe the adsorption process better (Table S1†). Although the adsorption mechanism cannot be directly determined from the fitted kinetic models,[31] the higher h value (eqn (S7)†) expressed by mg g^{-1} min^{-1}, the faster the adsorption rate of SMX. The h value increased at higher initial SMX concentrations (Table S1†) due to the stronger diffusion driving force. To further analyze the adsorption kinetic data, we have studied the data based on the intra-particle-diffusion model. Fig. 4b showed the intra-particle-diffusion model fit curve for SMX adsorption to 2K-700 at different initial

concentrations. As shown in Fig. 4b, the multi-linear curves showed that the whole process was a multi-step mechanism such as intraparticle diffusion and boundary layer diffusion. As the porous carbon surface was gradually saturated during the adsorption process, the rate constants decreased with time ($k_1 > k_2$, Table S2†).[32] As the initial SMX concentration increased, the values of k_1 gradually increased. At the same time, as the initial SMX concentration increased, the C_i value also increased gradually, which indicated that boundary layer diffusion was stronger.[33]

3.4. Effect of pH on adsorption

We investigated the effect of pH on adsorption of SMX with 2K-700. As shown in Fig. 5a, the change in pH had a significant effect on the amount of SMX adsorbed. According to previous reports,[34] the SMX molecule possesses two pKa values at 1.6 and 5.7. Therefore, SMX exists in three different forms in different pH solutions.[35] As shown in Fig. S6f,† according to the zeta potential results, the surface of 2K-700 was negatively charged at pH > 4.2, and the opposite was true at pH < 4.2. Therefore, at pH > 5.7, SMX had a negative charge. At the same time, since the pH was above 4.2 (isoelectric point of 2K-700), the surface of 2K-700 was also negatively charged (Fig. S6f†), resulting in a lower adsorption at high pH due to the presence of electrostatic repulsion between 2K-700 and SMX. At a lower pH (pH = 4.2), the surface of the 2K-700 was electrically neutral according to
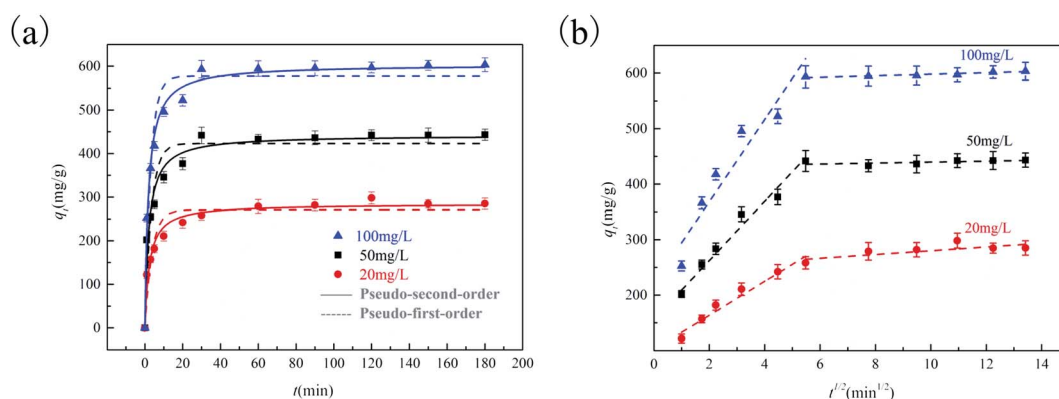

Fig. 4 Adsorption kinetics of SMX fitted by pseudo-first-order and pseudo-second-order rate model onto 2K-700 (a) and intra-particle diffusion fitting for adsorption of SMX onto 2K-700 (b).
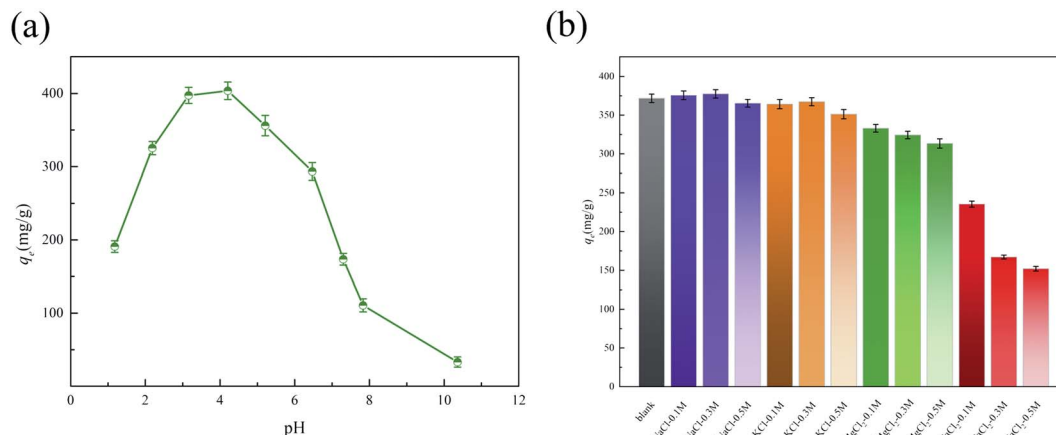
(a)

(b)

Fig. 5   Effect of pH on adsorption of SMX on 2K-700 (a) and effect of ionic strength on adsorption of SMX on 2K-700 (b).

the zeta potential. At this time, SMX was also electrically neutral (1.6 < pH < 5.7), resulting in a higher adsorption amount due to the disappearance of electrostatic repulsion. Further, when the pH was very low (pH < 1.6), we observed a significant decrease in the amount of adsorption. This might be due to the fact that both 2K-700 and SMX were positively charged, and electrostatic repulsion occurred again.

3.5.   Effect of ionic strength on adsorption

The antibiotics in the water pollution is usually associated with the presence of salt metal cations.[36] According to previous studies,[37] the presence of cations will affect the electrostatic interactions, thus significantly reducing the adsorption performance of adsorbents. In this study, the effects of four common cations Na^+, K^+, Mg^{2+} and Ca^{2+} (concentration 0.1, 0.3, 0.5 M) on the adsorption performance of 2K-700 for SMX were studied. As shown in the Fig. 5b, the adsorption performance did not change significantly when Na^+ and K^+ were added to the solution. This indicated that the electrostatic interaction was not the main adsorption mechanism. When Mg^{2+} or Ca^{2+} was added, the adsorption of SMX by 2K-700 decreased significantly. According to previous studies,[38] it was inferred that the complexation reaction between Mg^{2+} or Ca^{2+} and the functional groups on the carbon surface resulted in the decreased adsorption amount of SMX by 2K-700.

3.6.   Adsorption mechanism

Generally, the adsorption process was greatly affected by the textural characteristics of the adsorbent.[39] A structure–activity relationship between the SMX adsorption amount and S_{BET} of porous carbons was established (Fig. S7a†). There was a very obvious positive linear trend between q_{max} and S_{BET} ($R^2 = 0.98$). Based on previous reports,[39–41] we concluded that hydrophobic interactions and electron donor–acceptor (EDA) interactions were the main driving forces in the SMX adsorption process. Due to the large surface area of 2K-700, more active sites were provided for the interaction between SMX and 2K-700, which was advantageous for the hydrophobic adsorption of the SMX,

resulting in a greater amount of adsorption. In previous reports, SMX adsorption was also subjected to other important driving forces, which were most likely related to heteroatom functional groups on porous carbon.

The activated carbon in this study also had heteroatom functional groups. By plotting the relationship between q_{max}/S_{BET} and nitrogen content, we found that the no clear positive or negative relationship existed between the two values (Fig. S7b†). According to previous reports,[42] the formation of water clusters was related to the hydrophobicity of the adsorbent surface, and the presence of hydrophilic functional groups weakened the hydrophobicity of the porous carbon surface, which was clearly detrimental to the hydrophobic adsorption of SMX. In addition, different functional groups might also affect the intensity of EDA interaction between 2K-700 and SMX (Table 4).[43] On the one hand, both the pyridinic-N and the oxide-N were p-type dopants,[44,45] causing a decrease in the charge density of the carbon π-network, which was disadvantageous for the EDA interaction between the porous carbon surface and the SMX molecule. On the other hand, pyridinic-N and the oxide-N were hydrophilic groups, which were disadvantageous for the hydrophobic adsorption of porous carbon to SMX. For graphitic-N, the charge density increase of the carbon π-network was expected because the doping type of the graphitic-N is n-type doping.[44] Obviously, this is beneficial for the EDA interaction between the carbon surface and the SMX.[46] In

Table 4   Effect of heteroatoms on hydrophobic interactions and EDA interactions

Heteroatom	Hydrophobic interaction	EDA interaction
Pyridinic-N	−	−
Pyrrolic-N	−	+
Oxide-N	−	−
Graphitic-N	+	+
Carbonyl-O	−	−
Hydroxyl-O	−	+

addition, the graphitic-N was a hydrophobic group,[47] which was advantageous for the hydrophobic adsorption. Although pyrrolic-N is also a hydrophobic group, it could be slightly dissolved in water. Thus, the doping of pyrrolic-N could be an adverse effect on the hydrophobic adsorption of SMX. Besides, considering the electron donating property of pyrrolic-N,[45] it was advantageous for EDA interaction. For oxygen species, carbonyl-O was detrimental to both hydrophobic interactions and EDA interactions. Similar to pyrrolic-N, hydroxyl-O promoted EDA interaction but was detrimental to the hydrophobic adsorption of SMX by porous carbon. In short, the overall effect of heteroatoms on adsorption was found to be complex due to the multiple effects of diverse functional groups on the adsorption process.

3.7 Regeneration study and adsorption of SMX in lake water

Undoubtedly, the reusability of the adsorbent was very important for the cost control in practical applications. According to previous reports,[35,48] it was found that water does not effectively desorb SMX, and methanol or ethanol was an effective solvent. So, we used ethanol to wash and regenerate 2K-700 that had adsorbed SMX. Fig. S8† showed the recyclability of 2K-700 in SMX adsorption. After the first repeated use, the amount of SMX adsorption on 2K-700 was only 20% lower than that of the first use. The adsorption capacity tended to be stable from the second to fourth cycles, showing good reusability.

For potential practical applications, we further spiked SMX into the lake water to test the performance of 2K-700 in removing SMX from real water. The lake water used in the adsorption experiment was taken from the Pan lake of Tiangong University. The properties of the lake water used in this work are shown in Table S3.† As shown in Fig. S9,† q_{max} of SMX in lake water calculated from Langmuir model was 213.58 mg g^{-1} (Table S4†). First of all, natural water contains many natural organic matter (Table S3,† TOC = 8.25 mg L^{-1}). These NOMs may occupy some adsorption sites and compete with SMX.[49] Secondly, as discussed in Section 3.4, adsorption of SMX on 2K-700 was highly pH-dependent. The lake water was weakly alkaline (Table S3,† pH = 8.60), which may cause a decrease in the amount of adsorption. Finally, the decrease in adsorption capacity may also be caused by inorganic ions in the lake water (Table S3,† conductivity = 2.32 mS cm^{-1}) as discussed in Section 3.5.

4. Conclusions

Highly porous carbons obtained from EDTA-2K, EDTA-2Na and EDTA-4Na were prepared. The porous carbon materials prepared using potassium and sodium salt as precursors show significant differences in microscopic morphologies, pore structures and SMX adsorption capacities. The optimum adsorbent was obtained at 700 °C using EDTA-2K as the precursor. Compared with previous reports, 2K-700 and 2K-800 showed excellent adsorption capacity for SMX (Table S5†). A positive linear correlation was found between the adsorption capacities of SMX and S_{BET} of the carbons. Combination with

effects of pH and ionic strength, hydrophobic interaction and π–π EDA interaction were inferred to be the main adsorption mechanisms. Effects of various heteroatom groups on adsorption of SMX were analyzed in detail. It was inferred that graphitic-N should be favorable for the adsorption of SMX, while the presence of pyridinic-N, oxide-N or carbonyl-O could be unfavorable. The overall effect of functional groups on SMX adsorption was complex due to their multiple types. The reusability of the porous carbon was also investigated and found to be acceptable. Finally, the adsorption of SMX in lake water was also investigated, and the decrease in the adsorption amount was attributed to the high pH, competitive adsorption of NOM as well as inorganic ions in lake water. This work may provide valuable reference for future design of high-performance carbons for SMX adsorption from water.

Conflicts of interest

There are no conflicts of interest to declare.

Acknowledgements

References

1 A. K. Sarmah, M. T. Meyer and A. B. Boxall, *Chemosphere*, 2006, **65**, 725–759.

2 L. Zuo, J. Ai, H. Fu, W. Chen, S. Zheng, Z. Xu and D. Zhu, *Environ. Pollut.*, 2016, **211**, 425–434.

3 X. Wei, X. Bao, J. Wu, C. Li, Y. Shi, J. Chen, B. Lv and B. Zhu, *RSC Adv.*, 2018, **8**, 10396–10408.

4 W. Qi, H. Singer, M. Berg, B. Müller, B. Pernet-Coudrier, H. Liu and J. Qu, *Chemosphere*, 2015, **119**, 1054–1061.

5 J. Xu, Y. Xu, H. Wang, C. Guo, H. Qiu, Y. He, Y. Zhang, X. Li and W. Meng, *Chemosphere*, 2015, **119**, 1379–1385.

6 D. H. Carrales-Alvarado, R. Ocampo-Pérez, R. Leyva-Ramos and J. Rivera-Utrilla, *J. Colloid Interface Sci.*, 2014, **436**, 276–285.

7 M. Zbair, H. Ait Ahsaine and Z. Anfar, *J. Cleaner Prod.*, 2018, **202**, 571–581.

8 K. Yuan, C. Lu, S. Sfaelou, X. Liao, X. Zhuang, Y. Chen, U. Scherf and X. Feng, *Nano Energy*, 2019, **59**, 207–215.

9 M. A. Lillo-Ródenas, J. Juan-Juan, D. Cazorla-Amorós and A. Linares-Solano, *Carbon*, 2004, **42**, 1371–1375.

10 J. Wang and S. Kaskel, *J. Mater. Chem.*, 2012, **22**, 23710–23725.

11 B. Xu, H. Duan, M. Chu, G. Cao and Y. Yang, *J. Mater. Chem. A*, 2013, **1**, 4565–4570.

12 J. D. Atkinson and M. J. Rood, *Microporous Mesoporous Mater.*, 2012, **160**, 174–181.

13 M. Sevilla and A. B. Fuertes, *J. Mater. Chem. A*, 2013, **1**, 13738–13741.

14 J. He, J. Dai, A. Xie, S. Tian, Z. Chang, Y. Yan and P. Huo, *RSC Adv.*, 2016, **6**, 84536–84546.

15 F. Bonino, S. Brutti, P. Reale, B. Scrosati, L. Gherghel, J. Wu and K. Müllen, *Adv. Mater.*, 2005, **17**, 743–746.

16 J. Dai, S. Tian, Y. Jiang, Z. Chang, A. Xie, R. Zhang and Y. Yan, *J. Alloys Compd.*, 2018, **732**, 222–232.

17 P. Pachfule, D. Shinde, M. Majumder and Q. Xu, *Nat. Chem.*, 2016, **8**, 718–724.

18 S. Roldán, I. Villar, V. Ruíz, C. Blanco, M. Granda, R. Menéndez and R. Santamaría, *Energy Fuels*, 2010, **24**, 3422–3428.

19 A. Terracciano, J. Zhang, C. Christodoulatos, F. Wu and X. Meng, *J. Environ. Sci.*, 2017, **57**, 8–14.

20 Y. Shang, C. Chen, P. Zhang, Q. Yue, Y. Li, B. Gao and X. Xu, *Chem. Eng. J.*, 2019, **375**, 122004.

21 S. Zhu, X. Huang, F. Ma, L. Wang, X. Duan and S. Wang, *Environ. Sci. Technol.*, 2018, **52**, 8649–8658.

22 C. Lu, J. Yang, S. Wei, S. Bi, Y. Xia, M. Chen, Y. Hou, M. Qiu, C. Yuan, Y. Su, F. Zhang, H. Liang and X. Zhuang, *Adv. Funct. Mater.*, 2019, **29**, 1806884.

23 Y. Shi, G. Liu, L. Wang and X. Zhang, *Chem. Eng. J.*, 2015, **259**, 771–778.

24 P. Zhang, X. Mao and B. Yang, *Ind. Eng. Chem. Res.*, 2019, **58**, 10589–10598.

25 H. Li, Q. Deng, H. Chen, X. Cao, J. Zheng, Y. Zhong, P. Zhang, J. Wang, Z. Zeng and S. Deng, *Appl. Catal., A*, 2019, **580**, 178–185.

26 H. Kohay, I. I. Bilkis and Y. G. Mishael, *J. Colloid Interface Sci.*, 2019, **552**, 517–527.

27 W.-D. Oh, A. Veksha, X. Chen, R. Adnan, J.-W. Lim, K.-H. Leong and T.-T. Lim, *Chem. Eng. J.*, 2019, **374**, 947–957.

28 L. Wu, S. Sitamraju, J. Xiao, B. Liu, Z. Li, M. J. Janik and C. Song, *Chem. Eng. J.*, 2014, **242**, 211–219.

29 W. Chaikittisilp, K. Ariga and Y. Yamauchi, *J. Mater. Chem. A*, 2013, **1**, 14–19.

30 Y. Shi, G. Liu, L. Wang and H. Zhang, *RSC Adv.*, 2019, **9**, 17841–17851.

31 H. N. Tran, S. J. You, A. Hosseini-Bandegharaei and H. P. Chao, *Water Res.*, 2017, **120**, 88–116.

32 N. Farzin Nejad, E. Shams, M. K. Amini and J. C. Bennett, *Microporous Mesoporous Mater.*, 2013, **168**, 239–246.

33 X. Wei, Z. Zhang, L. Qin and J. Dai, *J. Taiwan Inst. Chem. Eng.*, 2019, **95**, 532–540.

34 A. K. Bajpai, M. Rajpoot and D. D. Mishra, *Colloids Surf., A*, 2000, **168**, 193–205.

35 I. Ahmed, B. N. Bhadra, H. J. Lee and S. H. Jhung, *Catal. Today*, 2018, **301**, 90–97.

36 M. E. Parolo, M. C. Savini, J. M. Vallés, M. T. Baschini and M. J. Avena, *Appl. Clay Sci.*, 2008, **40**, 179–186.

37 Y. Aldegs, M. Elbarghouthi, A. Elsheikh and G. Walker, *Dyes Pigm.*, 2008, **77**, 16–23.

38 J. Dai, A. Xie, R. Zhang, W. Ge, Z. Chang, S. Tian, C. Li and Y. Yan, *J. Mol. Liq.*, 2018, **256**, 203–212.

39 L. Nielsen, M. J. Biggs, W. Skinner and T. J. Bandosz, *Carbon*, 2014, **80**, 419–432.

40 M. Kah, G. Sigmund, F. Xiao and T. Hofmann, *Water Res.*, 2017, **124**, 673–692.

41 M. B. Ahmed, J. L. Zhou, H. H. Ngo, M. A. H. Johir, L. Sun, M. Asadullah and D. Belhaj, *J. Hazard. Mater.*, 2018, **360**, 270–278.

42 P. A. Quinlivan, L. Li and D. R. U. Knappe, *Water Res.*, 2005, **39**, 1663–1673.

43 Z. R. Ismagilov, A. E. Shalagina, O. Y. Podyacheva, A. V. Ischenko, L. S. Kibis, A. I. Boronin, Y. A. Chesalov, D. I. Kochubey, A. I. Romanenko, O. B. Anikeeva, T. I. Buryakov and E. N. Tkachev, *Carbon*, 2009, **47**, 1922–1929.

44 T. Schiros, D. Nordlund, L. Palova, D. Prezzi, L. Zhao, K. S. Kim, U. Wurstbauer, C. Gutierrez, D. Delongchamp, C. Jaye, D. Fischer, H. Ogasawara, L. G. Pettersson, D. R. Reichman, P. Kim, M. S. Hybertsen and A. N. Pasupathy, *Nano Lett.*, 2012, **12**, 4025–4031.

45 Q. Chen, J. Zheng, J. Xu, Z. Dang and L. Zhang, *Chem. Eng. J.*, 2019, **356**, 341–349.

46 C. L. Muhich, J. Y. Westcott, T. C. Morris, A. W. Weimer and C. B. Musgrave, *J. Phys. Chem. C*, 2013, **117**, 10523–10535.

47 M. Zhu, K. Zhou, X. Sun, Z. Zhao, Z. Tong and Z. Zhao, *Chem. Eng. J.*, 2017, **317**, 660–672.

48 R. Li, Y. Zhang, W. Chu, Z. Chen and J. Wang, *RSC Adv.*, 2018, **8**, 13546–13555.

49 C. Jung, J. Park, K. H. Lim, S. Park, J. Heo, N. Her, J. Oh, S. Yun and Y. Yoon, *J. Hazard. Mater.*, 2013, **263**, 702–710.